Ultrasonic imaging of highly scattering media from local measurements of the diffusion constant: Separation of coherent and incoherent intensities

Alexandre Aubry* and Arnaud Derode†
Laboratoire Ondes et Acoustique, ESPCI, Université Denis Diderot (Paris VII), CNRS (UMR 7587), 10 rue Vauquelin, 75005 Paris, France
(Received 27 September 2006; published 6 February 2007)

As classical imaging fails with diffusive media, one way to image a multiple-scattering medium is to achieve local measurements of the dynamic transport properties of a wave undergoing diffusion. This paper presents a method to obtain local measurements of the diffusion constant D in a multiple-scattering medium. The experimental setup consists in an array of programmable transducers placed in front of the multiple-scattering medium to be imaged. By achieving Gaussian beamforming both at emission and reception, an array of virtual sources and receivers located in the near field is constructed. The time evolution of the incoherent component of the intensity backscattered on this virtual array is shown to represent directly the growth of the diffusive halo as $\sqrt{Dt}$. A matrix treatment is proposed to separate the incoherent intensity from the coherent backscattering peak. Once the incoherent contribution is isolated, a local measurement of the diffusion constant is possible. The technique is applied to image the long-scale variations of D in a random-scattering sample made of two parts with a different concentration of cylindrical scatterers. This experimental result is obtained with ultrasonic waves around 3 MHz. It illustrates the possibility of imaging diffusive media from local measurements of the diffusion constant, based on coherent Gaussian beamforming and a matrix "antisymmetrization," which creates a virtual antireciprocity.

DOI: 10.1103/PhysRevE.75.026602 PACS number(s): 43.20.+g, 42.25.Dd, 43.35.+d, 46.65.+g

I. INTRODUCTION

Multiple scattering of waves concerns many domains of physics, ranging from optics or acoustics to solid-state physics, seismology, medical imaging, or telecommunications [1–14]. In an inhomogeneous medium where the wave celerity c depends on the spatial coordinates $\mathbf{r}$, it is a classical approach to consider a scattering sample as one realization of a random process, and study statistical parameters such as the mean, variance, and correlation of the field amplitude or intensity. Under this approach, several physical parameters are relevant to characterize wave propagation in scattering media: the scattering mean-free path l_e, the transport mean-free path l^*, the diffusion constant D, the absorption length l_{abs}. From an experimental point of view, these parameters can be measured by a variety of experiments. Some of them involve measurements of the ensemble-averaged field transmitted through a scattering layer [15–20]. One can also study the variations of the mean intensity with time ("time-of-flight" distribution) [20–24], and fit the result with a radiative transfer or a diffusive model. The coherent backscattering effect [25–29] can also be taken advantage of to measure the diffusion constant D and the transport mean-free path l^* [30,31]. The advantage of backscattering measurements is that they can be obtained even if only one side of the medium is accessible. Moreover, in a thick scattering sample ($L \gg l^*$ with L the medium thickness), the transmitted signal is much less energetic. As to classical imaging techniques, they fail when multiple scattering predominates. However, one can still hope to measure the long-scale spatial variations of the diffusive parameters and build a map. The resulting image would not be an image of the celerity $c(\mathbf{r})$ but e.g., of the diffusion constant $D(\mathbf{r})$ and would therefore have a different resolution. Indeed, an ideal image would give details with a length scale of the order of the correlation length ξ of the celerity fluctuations. Experimentally, in a highly scattering medium where diffuse fields are used to build an image, a map of the diffusion constant $D(\mathbf{r})$ would have a resolution of the order of the transport mean-free path l^*, at best. Intrinsically, the measurement of D cannot be exactly local, since the wave has to be scattered (hence, to travel over a distance $\mathcal{L}$ of the order of a few mean-free paths) before it makes sense to speak of wave diffusion. So there are essentially three length scales in ascending order: ξ, l^*, and $\mathcal{L}$. Even though classical imaging fails in diffusive media, one can try to build maps of D, with a resolution given by $\mathcal{L}$. This is similar to what can be done in seismology, where the coda Q factor is found to be a regional constant [9], or in medical imaging [13], where diffuse optical tomography is used to reconstruct the internal distribution of the reduced-scattering coefficient in the breast.

Here, we investigate the possibility of measuring spatial variations of the diffusion constant in a scattering medium, based on the mean dynamic backscattered intensity and near-field Gaussian beamforming. In acoustics, the diffusion constant D can be estimated from the coherent backscattering (CB) effect [30]. It is well known that dynamic CB is a signature of multiple scattering and manifests itself as a peak in the backscattered intensity with a typical angular width $\lambda/\sqrt{Dt}$. However, this result is only valid in the far field, when the source-sample distance a is very large compared to $\sqrt{Dt}$. In that case, the whole sample is illuminated by a quasiplane wave. In order to obtain a *local* measurement of D, the source can be brought close to the medium, but in that

*Electronic address: alexandre.aubry@espci.fr
†Electronic address: arnaud.derode@espci.fr

case, the angular width of the CB peak depends only on the wavelength and the source size [11,32], and brings no information on the diffusion constant. However, in the ensemble-averaged backscattered intensity, there are two contributions: the so-called coherent part (which is responsible for the CB peak) and the incoherent background. We show that, if the source and receivers are strongly directive (collimated beams) and located in the near-field, the incoherent intensity exhibits the growth of the diffusive halo with time: the width of the incoherent contribution does depend on the diffusion constant, unlike the coherent contribution. Basically, in a typical near-field experiment, the angular distribution of the backscattered intensity at a given time has the following shape: a narrow, steep peak (the coherent contribution), on top of a wider pedestal that widens with time (the incoherent contribution) (see Fig. 2). The problem is that it is difficult to distinguish between the coherent and the incoherent contributions, especially at early times. In addition, speckle fluctuations cannot be entirely averaged out by spatial averaging, in order to maintain a significant resolution.

In this paper, we present an experimental illustration of a method that allows one to separate the coherent and the incoherent contributions, and obtain a local measurement of the diffusion constant from the near-field backscattered intensity. The experiment utilizes programmable piezoelectric elements that transmit and receive ultrasound waves around 3 MHz. Gaussian beamforming is applied to incoming and outgoing wave fields, in order to create arrays of virtual sources and receivers at the surface of the sample. It is similar to seismic measurements [10] where geophones sit at the surface of the Earth, except that sources and receivers are not pointlike but strongly directive, as Gaussian beams are collimated. The source/receiver responses form a transfer matrix, which is symmetric because of reciprocity. Yet, this transfer matrix can be "made antisymmetric" to separate the coherent from the incoherent part. By "made antisymmetric," we mean that the upper matrix elements are kept unchanged while the diagonal elements are nulled and the sign of lower matrix elements is reversed. Once the coherent contribution is subtracted, the diffusion constant is retrieved by fitting the evolution of the incoherent contribution with time. The medium under investigation consists of two adjacent random collections of steel rods, with different densities (29 rods/cm^2 and 12 rods/cm^2), hence the diffusion constant is not homogeneous but shows long-scale variations. The spatial dependence of the diffusion constant is measured and exhibits a cutoff at the border between the two parts of the random-scattering sample. The experimental result shows the possibility of imaging random media based on local measurements of the diffusion constant.

II. NEAR-FIELD BEAMFORMING WITH GAUSSIAN BEAM

A. Experimental setup

The experiment takes place in a water tank. We use an N-element ultrasonic array ($N=128$) with a 3 MHz central frequency and a 2.5–3.5 MHz bandwidth; each array element is 0.39 mm in size and the array pitch p is 0.417 mm.

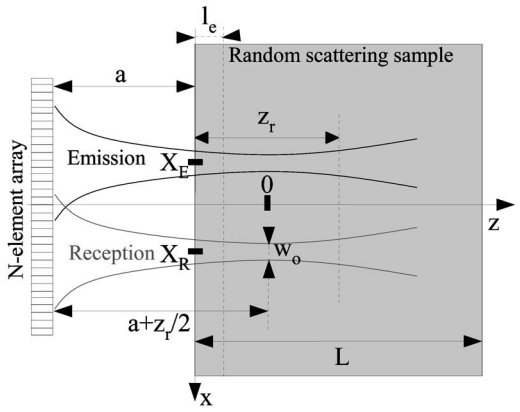

FIG. 1. Experimental setup: a 128-element linear array is placed in front of a random-scattering sample at a distance a. The whole setup is immersed in a water tank. The array is parallel to the scattering slab. Each array element is controlled by independent D/A and A/D converters. Gaussian beamforming allows one to send a collimated beam entering at $x=X_E$ in the emitting mode and to receive a collimated beam coming out at $x=X_R$ in the receiving mode. The beam is characterized by its waist width w_0 and the Rayleigh range z_r that defines the area where the Gaussian beam is collimated. The focal spot of the Gaussian beam is centered at a distance $z_r/2$ behind the surface of the scattering sample.

The sampling frequency is 20 MHz. The first step of the experiment consists in measuring the interelement matrix of the array (see Fig. 1). A 100-μs-long linear chirp is emitted from transducer i into the scattering sample immersed in water. The backscattered wave is then recorded with the N transducers of the same array. The operation is repeated for the N emitting transducers. The response from transducer i to transducer j is correlated with the emitted chirp, which gives the impulse response $h_{ij}(t)$. The $N\times N$ array response matrix $\mathbf{H}(t)$ whose elements are the N^2 impulse responses $h_{ij}(t)$ is thus obtained. Because of reciprocity, $h_{ij}(t)=h_{ji}(t)$ and $\mathbf{H}(t)$ is symmetric. A classical way to build the coherent backscattering cone is to calculate directly the angular distribution of the backscattered intensity by averaging $h_{ij}^2(t)$ over all pairs (i,j) separated by the same angle [30,31,33]. Here, as a local measurement of the diffusion constant is required, Gaussian beamforming is applied to the $\mathbf{H}$ matrix before computing the intensity.

B. Gaussian beam

A Gaussian beam can be expressed as [34]

$$\psi(x,z,k) = \sqrt{\frac{2}{\pi}}\frac{\exp\{j[\phi_0-\phi(z)]\}}{w(z)} \times\exp\left[-j\frac{kx^2}{2R(z)}-\frac{x^2}{w^2(z)}\right]\exp(jkz). \quad (1)$$

This expression describes the beam amplitude as a function of the transversal coordinate x and the axial coordinate z. k is the wave number. $w(z)$ is the beam width; its evolution along the direction of propagation z is

$$w(z) = w_0 \sqrt{1 + \left(\frac{z\lambda}{\pi w_0^2} \right)^2}. \quad (2)$$

The beam width $w(z)$ reaches its minimum value w_0 at $z=0$. This parameter w_0 is usually known as the beam waist width. $R(z)$ is the radius of curvature of the wave front of the Gaussian beam. Its dependence with z is as follows [34]:

$$R(z) = z\left[1 + \left(\frac{\pi w_0^2}{z\lambda} \right)^2 \right]. \quad (3)$$

$\phi(z)$ is known as the Guoy phase shift,

$$\phi(z) = \tan^{-1}\left(\frac{z}{z_r} \right). \quad (4)$$

z_r is the Rayleigh range [34],

$$z_r = \frac{\pi w_0^2}{\lambda}. \quad (5)$$

z_r gives the longitudinal dimension of the focal region; it is similar to the depth of field of a lens. In the region of the beam waist, the Gaussian beam can be considered as collimated and its expression simplifies into

$$\psi\left(x, -\frac{z_r}{2} < z < \frac{z_r}{2}, k \right) \simeq \sqrt{\frac{2}{\pi w_0^2}} \exp\left[-\frac{x^2}{w_0^2} \right] \exp(jkz). \quad (6)$$

Figure 1 depicts the Gaussian beams. As collimated beams are needed to obtain a simple expression of the incoherent intensity (see Sec. II D), the Gaussian beam is not focused exactly at the surface of the sample but at a distance of $z_r/2$ behind the surface, in order to maximize the range over which the Gaussian beam is collimated within the random medium.

C. Gaussian beamforming

To achieve Gaussian beamforming, the time signals $h_{ij}(t)$ are first truncated into 10-μs-long overlapping windows: $k_{ij}(T,t)=h_{ij}(T+t)W_R(t)$ with $W_R(t)=1$ for $t \in [0,10\ \mu s]$, $W_R(t)=0$ elsewhere. For each value of time T, the k_{ij} form a matrix $\mathbf{K}$. A short-time Fourier analysis is achieved by a fast-Fourier transform (FFT) and gives the response matrices $\mathbf{K}(T,f)$ at time T and frequency f. X_E and X_R are the transversal positions of Gaussian beams in emission and reception, respectively (see Fig. 1). From $\mathbf{K}(T,f)$, a virtual response matrix $\mathbf{K}^{GB}(T,f)$ is built; each of its elements $k^{GB}_{X_E,X_R}(T,f)$ correspond to the responses at the frequency f and time T between the emitted beam (at X_E) and the received beam (at X_R). The superscript GB stands for "Gaussian beamforming." The elements $k^{GB}_{X_E,X_R}(T,f)$ are calculated as follows:

$$k^{GB}_{X_E,X_R}(T,f) = \sum_{l=1}^{N}\sum_{m=1}^{N} k_{lm}(T,f)\psi\left(x_l - X_E, -a - z_r/2, \frac{2\pi f}{c} \right) \times \psi\left(x_m - X_R, -a - z_r/2, \frac{2\pi f}{c} \right). \quad (7)$$

N is the number of array elements. Equation (7) constitutes the Gaussian beamforming process.

With Parseval's theorem, the backscattered intensity $I^{GB}(X_E,X_R,T)$ can be obtained by integrating the squared norm of the responses $k^{GB}_{X_E,X_R}(T,f)$ over the frequency bandwidth (2.5–3.5 MHz). The results are averaged for all source/receiver couples that are separated by the same distance $X=|X_E-X_R|$. Thus, the averaged backscattered intensity $I^{GB}(X,T)$ after Gaussian beamforming is determined as

$$I^{GB}(X,T) = \langle |k^{GB}_{X_E,X_R}(T,f)|^2 \rangle_{f,\{X_E,X_R\}}, \quad (8)$$

where the symbol $\langle\ \rangle$ denotes an average over the variables in the subscript. This quantity is (ideally) the intensity that would have been obtained at time T with a Gaussian-shaped source and a Gaussian-shaped receiver separated by X and located at distance $z_r/2$ below the surface. The typical size of these virtual sources and receivers is controlled by the parameter w_0.

D. Expression of the coherent and incoherent intensities

In this subsection, the expressions of incoherent and coherent components of the intensity are determined from the theoretical studies by Akkermans *et al.* [27] (far field) and Margerin *et al.* [35] (near field) and applied to our experimental configuration. Let us introduce some notation. $\mathbf{R}_1(x_1,z_1)$ and $\mathbf{R}_n(x_n,z_n)$ are the position vectors of the first and last scatterer along a scattering path, respectively. The emitted beam is centered at $X_E=0$ for simplicity and the received beam at $X_R=X$. The emitted and backscattered beams $\psi_{in}(0,\mathbf{R}_1)$ and $\psi_{out}(\mathbf{R}_n,X)$ cannot be directly expressed with Eq. (6), because the presence of scatterers causes the wave packet to lose energy during the propagation through the random medium. As a consequence, on average, the emitted and backscattered beams decay spatially as $\exp[-(z+z_r/2)/(2l_e)]$, where l_e is the scattering mean-free path. Equation (6) is valid in the beam waist region. Thus, if the scattering mean-free path l_e is less than or equal to the Rayleigh length z_r, the first and last scattering events take place in the beam waist region. Then, the incident and backscattered beams $\psi_{in}(0,\mathbf{R}_1)$ and $\psi_{out}(\mathbf{R}_n,X)$ can be expressed as

$$\psi_{in}(0,\mathbf{R}_1) \simeq \sqrt{\frac{2}{\pi w_0^2}} \exp\left[-\frac{x_1^2}{w_0^2} \right] \times \exp\left[-\frac{(z_1 + z_r/2)}{2l_e} \right] \exp(jkz_1), \quad (9)$$

$$\psi_{out}(\mathbf{R}_n,X) \simeq \sqrt{\frac{2}{\pi w_0^2}} \exp\left[-\frac{(x_n-X)^2}{w_0^2}\right] \times \exp\left[-\frac{(z_n+z_r/2)}{2l_e}\right] \exp(jkz_n). \quad (10)$$

To model the diffusive propagation from $\mathbf{R}_1$ to $\mathbf{R}_n$, the Green's function for the intensity $P(\mathbf{R}_1,\mathbf{R}_n,T)$ in the random medium has to be introduced. $P(\mathbf{R}_1,\mathbf{R}_n,T)$ is the probability distribution to go from $\mathbf{R}_1$ to $\mathbf{R}_n$ in a time T for a random walker with the appropriate boundary conditions. For large lapse times, the Green function of the radiative transfer equation $P(\mathbf{R}_1,\mathbf{R}_n,T)$ can be approximated by the solution of the diffusion equation [36]. The expression of $P(\mathbf{R}_1,\mathbf{R}_n,T)$ for a semi-infinite medium [27] can be extended for a scattering slab [37] as follows:

$$P(\mathbf{R}_1,\mathbf{R}_n,T) = \frac{\exp\left[-\frac{(x_1-x_n)^2}{4DT}\right]}{\sqrt{4\pi DT}} \times \sum_{m=1}^{\infty} \sin\frac{m\pi(z_1+z_r/2+z_0)}{B} \times \sin\frac{m\pi(z_n+z_r/2+z_0)}{B} \exp\left(-\frac{m\pi^2 DT}{B}\right), \quad (11)$$

where z_0 comes from the exact solution of the Milne problem, which tells us that P cancels on the plane $z=-z_r/2-z_0$ with $z_0=\pi l^*/4$ (l^* is the transport mean-free path). $B=L+2z_0$ is the effective thickness of the medium. Finally, the incoherent and coherent intensities can be expressed as

$$I_{inc}(0,X,T) \simeq \int\int d^2\mathbf{R}_1 d^2\mathbf{R}_n |\psi_{in}(0,\mathbf{R}_1)|^2 P(\mathbf{R}_1,\mathbf{R}_n,T) \times |\psi_{out}(\mathbf{R}_n,X)|^2, \quad (12)$$

$$I_{coh}(0,X,T) \simeq \int\int d^2\mathbf{R}_1 d^2\mathbf{R}_n \psi_{in}(0,\mathbf{R}_1)\psi_{in}^*(0,\mathbf{R}_n) \times P(\mathbf{R}_1,\mathbf{R}_n,T)\psi_{out}(\mathbf{R}_1,X)\psi_{out}^*(\mathbf{R}_1,X). \quad (13)$$

Equations (12) and (13) neglect the propagation times before the first scattering and after the last scattering and are therefore valid when time T is much larger than the scattering mean-free time l_e/c. In Eqs. (9)–(11), the variables x_1 and x_n are separated from the variables z_1 and z_n. Thus, the calculation of integrals of Eqs. (12) and (13) is straightforward, and under the assumption $w_0^2 \ll 4DT$, the final results are

$$I_{inc}(0,X,T) \simeq (4\pi DT)^{-1/2} \exp\left(-\frac{X^2}{4DT}\right) I_z(T), \quad (14)$$

$$I_{coh}(0,X,T) \simeq (4\pi DT)^{-1/2} \exp\left(-\frac{X^2}{w_0^2}\right) I_z(T), \quad (15)$$

where $I_z(T)$ is the result of integrations on z_1 and z_n and is given by

$$I_z(T) = \sum_{m=1}^{\infty} \exp\left(-\frac{m\pi^2 DT}{B}\right) \left\{\left[\frac{1}{l_e^2}+\left(\frac{m\pi}{B}\right)^2\right]^{-1} \times \left[\frac{m\pi}{B}\cos\frac{m\pi z_0}{B}+\frac{1}{l_e}\sin\frac{m\pi z_0}{B}\right]\right\}^2. \quad (16)$$

The final expression of the incoherent intensity of Eq. (14) can be given a physical representation: the term $\exp\left(-\frac{X^2}{4DT}\right)$ represents the growth of the diffusive halo from which a local measurement of the diffusion constant may be obtained. The expression of the coherent intensity [Eq. (15)] shows that the width of the coherent backscattering peak does not display any time dependence, as the use of collimated beams at the surface of the sample corresponds to a near-field configuration. The typical width of the CB peak is therefore given by w_0. In this theoretical study, several assumptions have been made. First, the scattering mean-free path l_e has to be less than or equal to the Rayleigh length z_r in order to neglect the radius of curvature of the Gaussian beam. Second, the results of Eqs. (14) and (15) apply only for large times when the diffusion approximation of the radiative transfer equation is valid.

III. SEPARATION OF COHERENT AND INCOHERENT INTENSITIES

In order to achieve a local measurement of the diffusion constant from the growth of the diffusive halo, the incoherent and coherent intensities have to be separated. In this section, an original method is proposed. It relies on the "antisymmetrization" of the symmetric interelement matrix $\mathbf{H}(t)$ measured in the real space, which allows one to make a multiple-scattering path and its counterpart interferes destructively in the $\vec{k}$ space. Then, by achieving Gaussian beamforming on this antisymmetric matrix, the mean intensity [Eq. (8)] displays an "anticone" instead of the usual CB enhancement: the coherent intensity is subtracted rather than added to the incoherent intensity. Then, both intensities can be deduced from the cone and its "anticone."

A. Principle

Let us assume for simplicity that the interelement impulse responses $h_{ij}(t)$ are totally decorrelated one from each other. From Eqs. (7) and (8) the following expression for the averaged backscattered intensity after Gaussian beamforming $I^{GB}(X,T)$ is obtained:

$$I^{GB}(X,T) = \sum_{l_1=1}^{N}\sum_{m_1=1}^{N}\sum_{l_2=1}^{N}\sum_{m_2=1}^{N} \langle k_{l_1,m_1}(T,f)k_{l_2,m_2}^*(T,f)\psi_{l_1,E}(f) \times \psi_{m_1,R}(f)\psi_{l_2,E}^*(f)\psi_{m_2,R}^*(f)\rangle_{f,\{X_E,X_R\}}, \quad (17)$$

where $\psi_{l,E}(f)=\psi\left(x_l-X_E,-a-z_r/2,\frac{2\pi f}{c}\right)$. Because of the deco-

rrelation assumption and reciprocity, only the terms containing the products $k_{l_1,m_1}(T,f)k^*_{l_1,m_1}(T,f)$ and $k_{m_1,l_1}(T,f)k^*_{l_1,m_1}(T,f)$ survive the average. The first product consists of an incoherent summation of multiple-scattering-paths intensity: it corresponds to the incoherent intensity. The second one results from interference between multiple-scattering paths and their reciprocal counterparts: it is linked to the coherent intensity. Finally, the incoherent (I^{GB}_{inc}) and coherent intensities (I^{GB}_{coh}) after Gaussian beamforming are given by

$$I^{GB}_{inc}(X,T) = \sum_{l_1=1}^{N}\sum_{m_1=1}^{N} \langle |k_{l_1,m_1}(T,f)\psi_{l_1,E}(f)\psi_{m_1,R}(f)|^2\rangle_{f,\{X_E,X_R\}}, \tag{18}$$

$$I^{GB}_{coh}(X,T) = \sum_{l_1=1}^{N}\sum_{m_1=1}^{N} \langle k_{l_1,m_1}(T,f)k^*_{m_1,l_1}(T,f)\psi_{l_1,E}(f) \times \psi_{m_1,R}(f)\psi^*_{m_1,E}(f)\psi^*_{l_1,R}(f)\rangle_{f,\{X_E,X_R\}}. \tag{19}$$

If the reciprocity symmetry is respected, the interelement matrix $\mathbf{H}(t)$ is symmetric. From $\mathbf{H}(t)$, an antisymmetric matrix $\mathbf{H}^A(t)$ can be defined as follows:

(1) for $i<j$, $h^A_{ij}=h_{ij}$;
(2) for $i=j$, $h^A_{ii}=0$;
(3) for $i>j$, $h^A_{ij}=-h_{ij}$.

By replacing the measured responses $k_{ij}(T,f)$ by the fictitious responses $k^A_{ij}(T,f)$ in Eqs. (18) and (19), the incoherent ($I^{GB,A}_{inc}$) and coherent ($I^{GB,A}_{coh}$) intensities obtained from $\mathbf{H}^A(t)$ can be expressed as

$$I^{GB,A}_{inc}(X,T) = I^{GB}_{inc}(X,T) - \sum_{l_1=1}^{N} \langle |k_{l_1,l_1}(T,f)\psi_{l_1,E}(f)\psi_{l_1,R}(f)|^2\rangle_{f,\{X_E,X_R\}}, \tag{20}$$

$$I^{GB,A}_{coh}(X,T) = -I^{GB}_{coh}(X,t) + \sum_{l_1=1}^{N} \langle |k_{l_1,l_1}(T,f)\psi_{l_1,E}(f)\psi_{l_1,R}(f)|^2\rangle_{f,\{X_E,X_R\}}. \tag{21}$$

The physical (and fictitious) interpretation of the "antisymmetrization" procedure would be to build an antireciprocal medium, i.e., a medium for which the impulse responses from i to j and j to i are exactly out of phase ($h^A_{ij}=-h^A_{ji}$). In such a medium, there would be no coherent backscattering cone, but an "anticone" instead, at exact backscattering. Indeed, the interference between any multiple-scattering path and its reciprocal counterpart, which is represented by the product $k_{i,j}(T,f)k^*_{j,i}(T,f)$in Eq. (19), would be destructive. As a result, the coherent intensity obtained from H^A [Eq. (21)] is equal to the opposite of that obtained from the symmetric matrix H plus a residual term, due to the nulling of the diagonal terms. As the incoherent intensity corresponds to the summation of the individual intensities of multiple-scattering paths, the minus sign between h^A_{ij} and h^A_{ji} has no influence on $I^{GB,A}_{inc}$, which remains equal to I^{GB}_{inc}, except for the same residual term. Finally, when the total (coherent+incoherent) backscattered intensity $I^{GB,A}$ is calculated, the residual term vanishes and $I^{GB,A}$ is given by

$$I^{GB,A} = I^{GB,A}_{inc} + I^{GB,A}_{coh} = I^{GB}_{inc} - I^{GB}_{coh}. \tag{22}$$

Even though the antireciprocal medium has no physical existence, from a mathematical point of view the advantage of this trick is to separate the coherent and incoherent contributions in the intensity backscattered from the *real* medium. The incoherent and coherent intensities are obtained by summing and subtracting, respectively, the intensities corresponding to the symmetric (experimental) and the antisymmetric (fictitious) cases.

$$I^{GB}_{inc} = \frac{I^{GB} + I^{GB,A}}{2}, \tag{23}$$

$$I^{GB}_{coh} = \frac{I^{GB} - I^{GB,A}}{2}. \tag{24}$$

Actually, in the simple case of Gaussian beams, the separation of the coherent and incoherent terms could have been achieved more simply. Since the waist width w_0 is known, from Eq. (15) one can easily calculate and subtract the coherent part from the total intensity. Nevertheless, as it is shown in Sec. III B, the coherent backscattering peak width is slightly larger than w_0 because of the size of the array elements, so a direct subtraction of the coherent part would have been a possible source of error. The advantage of the antisymmetrization technique is that it does not require the beam to be Gaussian. It can be generalized to any kind of illumination. However, it relies on the assumption that the responses h_{lm} are fully decorrelated (or at least, have a finite correlation length), which is not the case when single scattering dominates. The antisymmetrization technique can successfully separate the coherent and the incoherent contributions to the total intensity only at times such that the single-scattering intensity can be neglected compared to the multiple-scattering contribution.

B. Experimental results

The experimental setup is shown in Fig. 1. The experimental process has already been described in Sec. II A. The distance a is 27.5 mm. An array of $N=128$ elements has been used. The random-scattering sample consists of steel rods ($C_L=5.7$ mm/μs, $C_T=3$ mm/μs, radius 0.4 mm, density 7.85 kg/l) randomly distributed with a concentration $n=29.54$ rods/cm^2. The frequency-averaged elastic mean-free path l_e is 3.15 ± 0.15 mm for this medium between 2.5 and 3.5 MHz [17]. Once the interelement matrix $\mathbf{H}$ is measured, the averaged backscattered intensity obtained with Gaussian beamforming $I^{GB}(X,T)$ is calculated as described in Sec. II C. The virtual array obtained with Gaussian beamforming contains 43 virtual elements, which correspond to the axial position of the collimated beams. The pitch p' of this virtual array is 1 mm. The beam waist width w_0 is 1 mm. The cor-

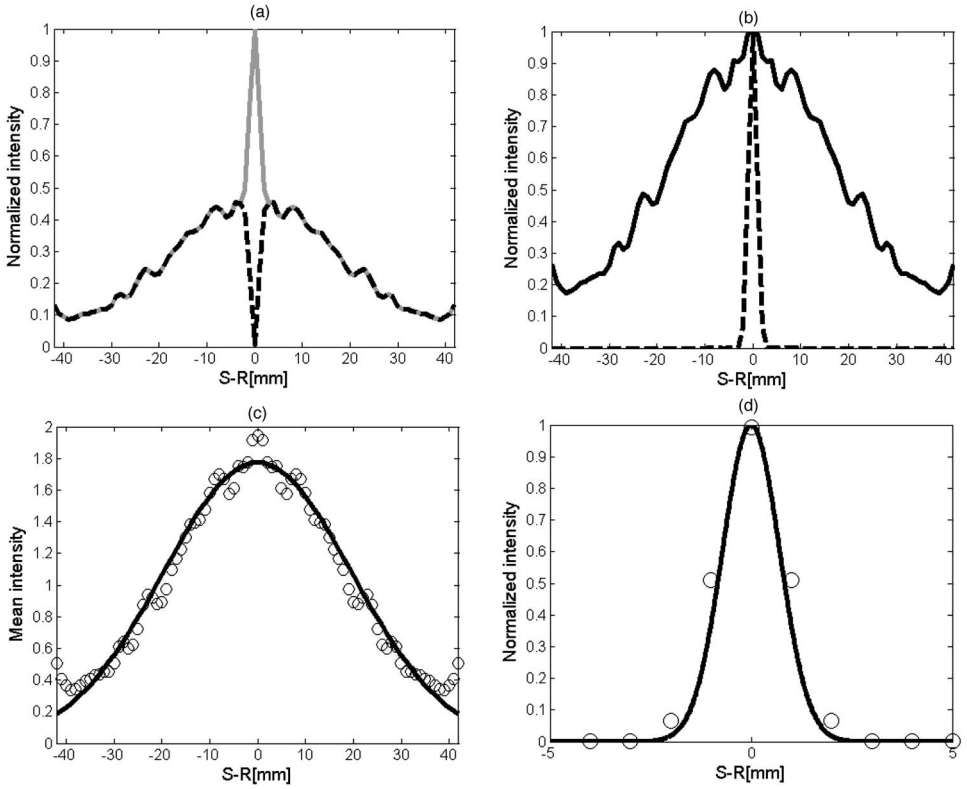

FIG. 2. Separation of the coherent and incoherent intensities. (a) Backscattered intensity obtained after Gaussian beamforming performed on matrix **H** (gray continuous line) and the antisymmetric matrix $\mathbf{H}^{\mathbf{A}}$ (dark dashed line). (b) Incoherent (continuous line) and coherent (dashed line) intensities obtained from the cone and "anticone" displayed in (a). (c) The incoherent intensity (circles) is fitted with a Gaussian curve (continuous line) whose variance W^2 allows one to determine the diffusion constant D. (d) The coherent intensity (circles) is compared to its theoretical expression (continuous line) given by Eq. (15).

responding intensity profile obtained at $T=70$ μs is shown in Fig. 2(a). The total intensity contains the incoherent intensity, which spreads far from the source, and the coherent intensity, which is only observed near the source. From this intensity distribution, the separation between the coherent and incoherent intensities is difficult. As a consequence, the "antisymmetrization" method described in the previous subsection is applied. The interelement matrix **H** is made antisymmetric and the corresponding intensity $I^{GB,A}(X,T)$ is shown in Fig. 2(a). An "anticone" is obtained as it is predicted by Eq. (22). Then, the addition and subtraction of $I^{GB}(X,T)$ and $I^{GB,A}(X,T)$ give access to the incoherent and coherent intensities [Fig. 2(b)]. The incoherent intensity looks like a Gaussian curve as it is predicted by Eq. (14), the residual fluctuations are due to a lack of averaging. The coherent intensity profile is compared to its theoretical expression [Eq. (15)] in Fig. 2(d). The experimental result and the theoretical prediction are in a good agreement. The small mismatch comes from the fact that transducers are not point-like sources and so the continuous approach used in Sec. II D does not model perfectly the experimental conditions.

IV. LOCAL MEASUREMENT OF THE DIFFUSION CONSTANT

In this section, local measurements of the diffusion constant D are achieved, based on Gaussian beamforming and the "antisymmetrization" technique. To this end, a random scattering sample containing two parts with different concentrations of scatterers has been used (see Fig. 3). The first sample consists of steel rods randomly distributed with a concentration $n_1=12$ rods/cm^2. The frequency-averaged scattering mean-free path l_1^e is 7.7 ± 0.3 mm for this medium between 2.5 and 3.5 MHz [17]. The second sample consists of the same steel rods but with a concentration $n_2=29.54$ rods/cm^2. The corresponding scattering mean-free path is $l_2^e=3.15\pm0.15$ mm [17]. The array sample distance a is 27.5 mm.

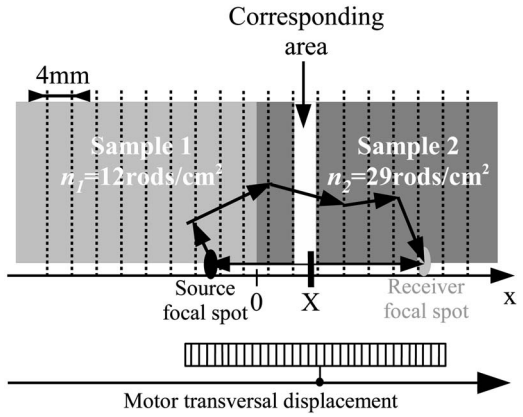

FIG. 3. Experimental process used to obtain a local measurement of the diffusion constant D. Two scattering samples are placed side by side in front of the 128-element array. These two samples differ by their concentrations in steel rods. The array can be moved with a motor. The space is divided into areas of 4 mm width. When a Gaussian beam is emitted at $x=X_E$ and received at $x=X_R$, the measured backscattered intensity is attributed to the area that contains $X=(X_E+X_R)/2$.

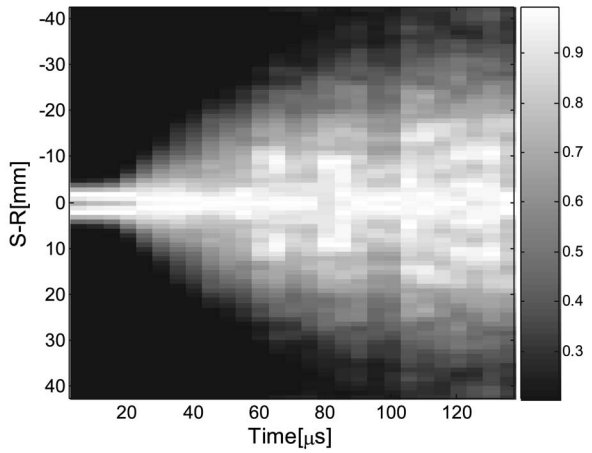

FIG. 4. Incoherent intensity corresponding to the area located at $X=+10$ mm. The intensity is normalized with its maximum at each time.

A. Experimental process

We use Gaussian beamforming to mimic a virtual array of 43 sources/receivers with a 1 mm pitch, for each position of the real array. The Gaussian beam waist width w_0 is 1 mm. The real 128-element array can be moved parallel to the front face of the sample with a motor. The experimental procedure is divided into four steps:

(1) The interelement matrix $\mathbf{H}(t)$ is recorded.

(2) The emission/reception on every point of the virtual array is calculated in the computer and yields $\mathbf{H}^{GB}(X_E,X_R)$.

(3) The antisymmetrization technique is applied to obtain the incoherent contribution of the backscattered intensity.

(4) The 128-element array is translated by 0.72 mm and the same procedure is repeated.

The region to image has been divided into 4-mm-wide areas (see Fig. 3). The aim is to obtain a measurement of D, at the scale of 4 mm, by a fit of the incoherent contribution. The inversion procedure is very crude: when a Gaussian beam is focused at X_E (in emission) and X_R (in reception), the resulting diffusive halo is attributed to the area with a spatial coordinate $X=(X_E+X_R)/2$. The diffusive halos corresponding to the same area are averaged, in order to reduce the speckle fluctuations. A typical example is represented in Fig. 4, where the growth of the averaged halo with time is obvious.

B. Experimental results

At each time, the incoherent intensity profile has been fitted with a Gaussian curve with a variance W^2. Figure 2(c) depicts an example of fit of the incoherent intensity at a given time. The best value W^2 is chosen such that the scalar product between the normalized Gaussian curve and normalized data is maximum. The model described in Sec. II D predicts that the temporal evolution of $W^2(T)$ should be equal to $2DT$. Thus, a linear fit of $W^2(T)$ gives access to the diffusion constant D. In Fig. 5, the temporal evolution of W^2 is shown for the two areas located at $X=-10$ mm (low-concentrated sample) and at $X=+10$ mm (high-concentrated sample). At $X=-10$ mm, the measured diffusion constant is 3.9 mm$^2/\mu$s, whereas at $X=+10$ mm, the diffusion constant is 2.4 mm$^2/\mu$s. This is not surprising: the diffusion constant decreases with the concentration of scatterers. Note that the linear fit is applied from $T=60$ μs only, which corresponds to a typical penetration depth of $6l_1^e$. Before this time, the diffusion approximation is not valid yet and the evolution of W^2 is not linear. Even if the condition $l_e<z_r$ is not strictly fulfilled for medium 1($X<0$), the experimental results shows that the model is still valid if l_e and z_r are of the same order of magnitude. The same data processing has been applied to each area and the spatial evolution of the diffusion constant D has been obtained and is shown in Fig. 6. A cutoff of the diffusion constant is observed at the border between the

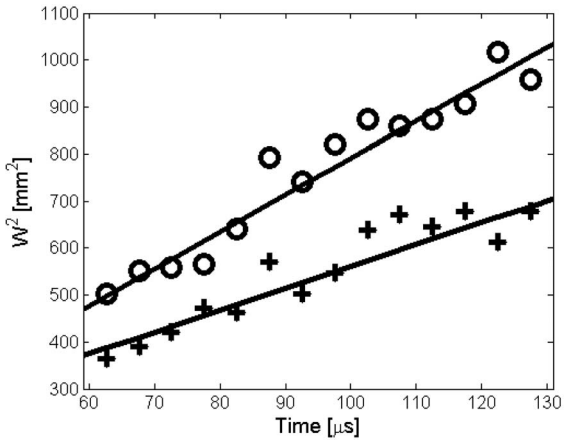

FIG. 5. Temporal evolution of the variance W^2 of the Gaussian curve, which fits the incoherent intensity profile from $T=60$ μs to $T=130$ μs. The circles correspond to the area located at $X=-10$ mm (low-concentrated sample) and the crosses to the area located at $X=+10$ mm (high-concentrated sample). A linear fit of W^2 is performed in each case (continuous lines) and provides a measurement of the diffusion constant. For $X=-10$ mm, the measured diffusion constant is $D=3.9$ mm$^2/\mu$s, whereas, for $X=+10$ mm, the measured diffusion constant is $D=2.4$ mm$^2/\mu$s.

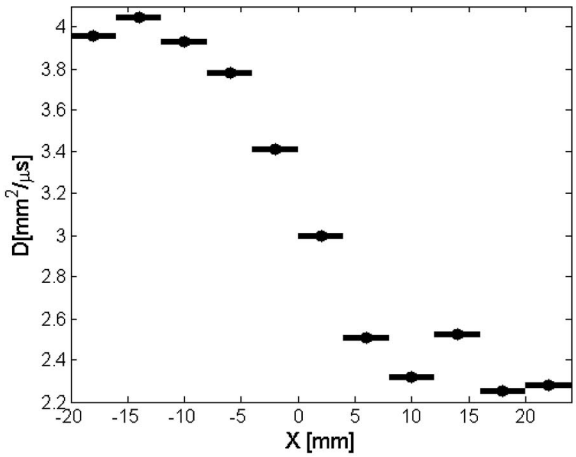

FIG. 6. Spatial evolution of the measured diffusion constant. For each area, the diffusion constant has been estimated and is plotted as a function of the lateral position X.

high-concentrated and the low-concentrated parts ($X=0$). The diffusion constant is about 4.0 $mm^2/\mu s$ for the low-concentrated medium and 2.4 $mm^2/\mu s$ for the high-concentrated one. The spatial resolution is intrinsically limited by the transport mean-free path l^*. Here, the transition for the diffusion constant spreads over 10 mm, which gives an order of magnitude for the spatial resolution of such a measurement. A better resolution would be obtained if the spatial mesh was denser. But, in this case, the average of the backscattered intensity would not be satisfying: residual fluctuations of the intensity pattern would be too high because of the lack of average over disorder configurations. Consequently, a compromise has to be found between the density of the mesh and a sufficient average over disorder configurations. Moreover, the spatial resolution is limited by the spreading of the diffusive halo characterized by the typical length $\mathcal{L}$: near the border ($X=0$), the diffusive halo spreads in both media, so the measured diffusion constant corresponds to an average of the diffusion constants of both media. The method proposed in this study does not allow one to achieve a three-dimensional image of a diffusive medium. Indeed, the medium is supposed to be homogeneous in the direction of depth (z) to achieve a local measurement of the diffusion constant $D(x,y)$ at the scale of $\mathcal{L}$. Yet this technique could provide a two-dimensional (2D) map of a diffusive medium from backscattered measurements taken at its surface.

V. CONCLUSION

In this study, we have investigated the possibility to measure locally the diffusion constant of an acoustic pulsed wave propagating in a strongly disordered 2D medium. To this end, Gaussian beamforming has been used and allows one to observe the local growth of the diffusive halo via the incoherent intensity. An original method to separate the coherent and incoherent intensities has been presented and applied to the case of ultrasonic waves. This method is based on the "antisymmetrization" of the interelement matrix; it creates an artificial antireciprocity, which allows one to separate the coherent backscattering peak from the incoherent background. The technique proposed in this paper has been applied experimentally to the observation of a gradient of concentration in scatterers from the spatial evolution of the diffusion constant. Experimental results are very encouraging and show that this technique would be of great interest to achieve 2D imaging of real multiple-scattering media.

ACKNOWLEDGMENTS

The authors would like to thank Dr. Julien de Rosny for fruitful discussions and Dr. Victor Mamou who made the steel rods samples. They also wish to acknowledge the groupe de recherches IMCODE of CNRS (GDR 2253).

[1] P. Sheng, *Scattering and Localization of Classical Waves in Random Media* (World Scientific, Singapore, 1990).
[2] P. Sheng, *Introduction to Wave Scattering, Localization and Mesoscopic Phenomena* (Academic Press, New York, 1995).
[3] A. Ishimaru, *Wave Propagation and Scattering in Random Media* (Academic Press, New York, 1978).
[4] P. Anderson, Phys. Rev. **109**, 1492 (1958).
[5] M. Rossum and T. Nieuwenhuizen, Rev. Mod. Phys. **71**, 313 (1999).
[6] A. Lagendijk and B. van Tiggelen, Phys. Rep. **270**, 143 (1996).
[7] P. Sebbah, *Waves and Imaging Through Complex Media* (Kluwer Academic Publishers, Dordrecht (Netherlands), 1999).
[8] A. Tourin, A. Derode, and M. Fink, Waves Random Media **10**, R31 (2000).
[9] K. Aki and B. Chouet, J. Geophys. Res. **80**, 3322 (1975).
[10] E. Larose, L. Margerin, B. van Tiggelen, and M. Campillo, Phys. Rev. Lett. **93**, 048501 (2004).
[11] B. van Tiggelen, L. Margerin, and M. Campillo, J. Acoust. Soc. Am. **110**, 1291 (2001).
[12] A. Yodh and B. Chance, Phys. Today **48**, 33 (1995).
[13] R. Choe, A. Corlu, K. Lee, T. Durduran, S. Donecky, M. Grosicka-Koptyra, S. Arridge, B. Czerniecki, D. Fraker, and A. DeMichele *et al.*, Med. Phys. **32**, 1128 (2005).
[14] A. Derode, A. Tourin, J. de Rosny, M. Tanter, S. Yon, and M. Fink, Phys. Rev. Lett. **90**, 014301 (2003).
[15] J. Page, P. Sheng, H. Sriemer, I. Jones, X. Jing, and D. Weitz, Science **271**, 634 (1996).
[16] Z. Zhang, I. Jones, H. Shriemer, J. Page, D. Weitz, and P. Sheng, Phys. Rev. E **60**, 4843 (1999).
[17] A. Derode, V. Mamou, and A. Tourin, Phys. Rev. E **74**, 036606 (2006).
[18] J. Scales and K. van Wijk, Appl. Phys. Lett. **79**, 2294 (2001).
[19] J. Scales and A. Malcolm, Phys. Rev. E **67**, 046618 (2003).
[20] M. Haney, K. van Wijk, and R. Snieder, Geophysics **70**, 1 (2005).
[21] J. Page, H. Shriemmer, A. Bailey, and D. Weitz, Phys. Rev. E **52**, 3106 (1995).
[22] S. Skipetrov and B. van Tiggelen, Phys. Rev. Lett. **92**, 113901 (2004).
[23] M. Storzer, P. Gross, C. Aegerter, and G. Maret, Phys. Rev. Lett. **96**, 063904 (2006).
[24] L. Margerin, M. Campillo, and B. van Tiggelen, Geophys. J. Int. **134**, 596 (1998).
[25] E. Akkermans, P.-E. Wolf, and R. Maynard, Phys. Rev. Lett. **56**, 1471 (1986).
[26] P.-E. Wolf and G. Maret, Phys. Rev. Lett. **55**, 2696 (1985).
[27] E. Akkermans, P.-E. Wolf, R. Maynard, and G. Maret, J. Phys. (France) **49**, 77 (1988).
[28] G. Labeyrie, F. de Tomasi, J.-C. Bernard, C. Müller, C. Miniatura, and R. Kaiser, Phys. Rev. Lett. **83**, 5266 (1999).
[29] R. Weaver and O. Lobkis, Phys. Rev. Lett. **84**, 4942 (2000).
[30] A. Tourin, A. Derode, P. Roux, B. van Tiggelen, and M. Fink, Phys. Rev. Lett. **79**, 3637 (1997).
[31] A. Tourin, A. Derode, A. Peyre, and M. Fink, J. Acoust. Soc.

Am. **108**, 503 (2000).
[32] J. de Rosny, A. Tourin, and M. Fink, Phys. Rev. Lett. **84**, 1693 (2000).
[33] A. Derode, V. Mamou, F. Padilla, F. Jenson, and P. Laugier, Appl. Phys. Lett. **87**, 114101 (2005).
[34] J. Alda, *Encyclopedia of Optical Engineering* (Taylor & Francis Group, New York, 2003), pp. 999–1013.
[35] L. Margerin, M. Campillo, and B. van Tiggelen, Geophys. J. Int. **145**, 593 (2001).
[36] J. Paasschens, Phys. Rev. E **56**, 1135 (1997).
[37] V. Mamou, Ph.D. dissertation (in French), Université Paris 7-Denis Diderot, 2005 (http://tel.archives-ouvertes.fr).